PERGAMON

International Journal of Solids and Structures 36 (1999) 3497–3516

INTERNATIONAL JOURNAL OF SOLIDS and STRUCTURES

Determining material true stress–strain curve from tensile specimens with rectangular cross-section

Z. L. Zhang*, M. Hauge, J. Ødegård, C. Thaulow

SINTEF Materials Technology, Rich. Birkelands vei 1C, N-7034 Trondheim, Norway

Received 22 November 1997; in revised form 23 April 1998

Abstract

The uniaxial true stress logarithmic strain curve for a thick section can be determined from the load–diameter reduction record of a round tensile specimen. The correction of the true stress for necking can be performed by using the well-known Bridgman equation. For thin sections, it is more practical to use specimens with rectangular cross-section. However, there is no established method to determine the complete true stress–logarithmic strain relation from a rectangular specimen. In this paper, an extensive three-dimensional numerical study has been carried out on the diffuse necking behaviour of tensile specimens made of isotropic materials with rectangular cross-section, and an approximate relation is established between the area reduction of the minimum cross-section and the measured thickness reduction. It is found that the area reduction can be normalized by the uniaxial strain at maximum load which represents the material hardening and also the section aspect ratio. Furthermore, for the same material, specimens with different aspect ratio give exactly the same true average stress–logarithmic strain curve. This finding implies that Bridgman's correction can still be used for necking correction of the true average stress obtained from rectangular specimens. Based on this finding, a method for determining the true stress–logarithmic strain relation from the load–thickness reduction curve of specimens with rectangular cross-section is proposed.

Keywords: Fracture; True stress–strain curve; Rectangular tensile specimen; Diffuse necking; Plastic forming; Bridging correction

Nomenclature

$\bar{\sigma}$	flow stress used as input for the finite element analyses
σ_E	'exact' true average stress obtained directly from the finite element results
σ_a	approximate true average stress calculated according to the proposed equation from the load–thickness reduction curve
$\bar{\sigma}_a$	Bridgman corrected true stress from the σ_a
S	cross-section aspect ratio

* Corresponding author. Fax: 00 47 73 59 29 31; E-mail: zhiliang.zhang@matek.sintef.no

0020–7683/99/$ - see front matter
PII: S0020–7683(98)00153–X

$\Delta A/A_0$	total area reduction ratio
$\Delta t/t_0$	thickness reduction ratio
$P_{\max}$	maximum load
A_0	initial area of the cross-section
A	current area of the cross-section
ε	logarithmic strain, $\varepsilon = \ln(A_0/A)$
t_0	initial thickness
ΔA_P	area reduction ratio due to proportional deformation
ΔA_S	area reduction ratio due to shape change of the cross-section

1. Introduction

True stress–logarithmic strain curve including material response in both the pre- and post-plastic localization regime, becomes essential when large deformation is considered, for example, in the metal forming analysis and in the analysis of ductile damage and fracture. It is also important in those cases where plastic strain hardening mismatch effect on the ductile behaviour is concerned. For thick sections, the true stress–logarithmic strain curve can usually be conveniently determined from the load–diameter reduction curve of round tensile bars, and the well known Bridgman (1952) equation can be used for necking correction. When thin sections are concerned, it is more practical to use specimens with rectangular cross-section for uniaxial tensile test. However, there is no method available for determining the whole true stress–logarithmic strain curve using rectangular specimens and the correction of the true stress for necking was thought to be more complicated than for the round bar. There are basically two problems in developing the method. The first problem is how to calculate or measure the true area, which is not only a function of loading, but also depends on section's aspect ratio and material's plastic hardening. According to the authors' knowledge, there is no practical measuring system available in the market to simultaneously measure the minimum true area of cross-section vs loading. The second problem is how to correct the true stress obtained from rectangular tensile specimen for necking, as it is obvious that the so-called true stress is the 'true average tensile stress' in the neck where the stress distribution is not uniform (see e.g. Aronofsky, 1951) and it should be corrected before it can be used as the uniaxial flow stress.

In a uniaxial tension test with ductile rate-independent material, plastic instability and flow localization will occur just after the maximum load and the so-called diffuse necking starts. This form of unstable flow is analogous to the neck formed in a round tensile bar. Diffuse necking may terminate in fracture. But usually after the onset of the diffuse neck, the deformation continues under the falling load until the development of a localized neck, which leads ultimately to ductile fracture (see e.g. Dieter, 1986; Bayoumi and Joshi, 1992). Figure 1 depicts the two types of necking observed in the uniaxial tension test with rectangular cross-section specimens. For specimens with low cross-section aspect ratio and strong plastic hardening ability, the localized neck can occur inclined at an angle to the tension axis, across the thickness of the specimen (Ødegård, 1997). The so-called sheet necking with a through thickness neck, inclined to the tension axis across the width of the specimen can be observed for specimens with high cross-section aspect ratio and low hardening ability. Figure 2 schematically shows the typical load vs displacement curve of a tension

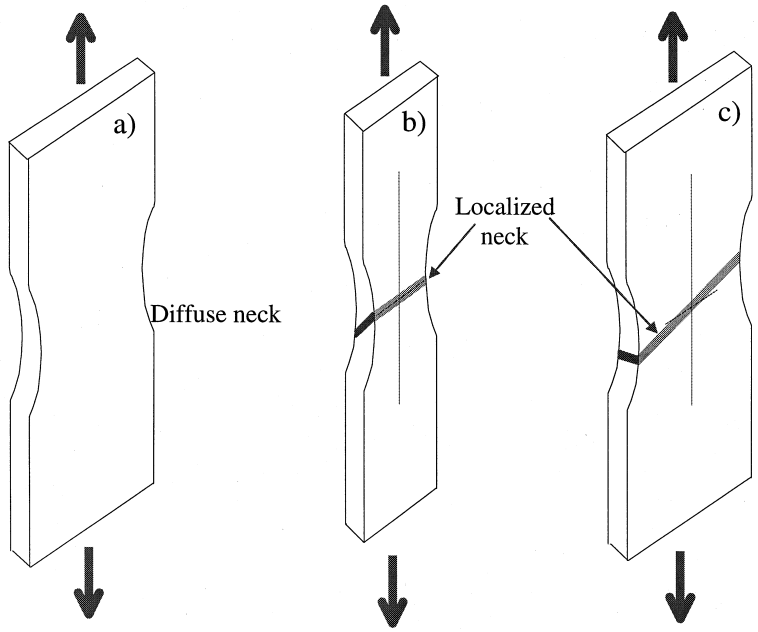

Fig. 1. Two types of necking in uniaxial tension using specimens with rectangular cross-section: diffuse necking (a), followed by local necking (b) for low aspect ratio and strong hardening and (c) for high aspect ratio and low hardening. The localized neck leads to final fracture.

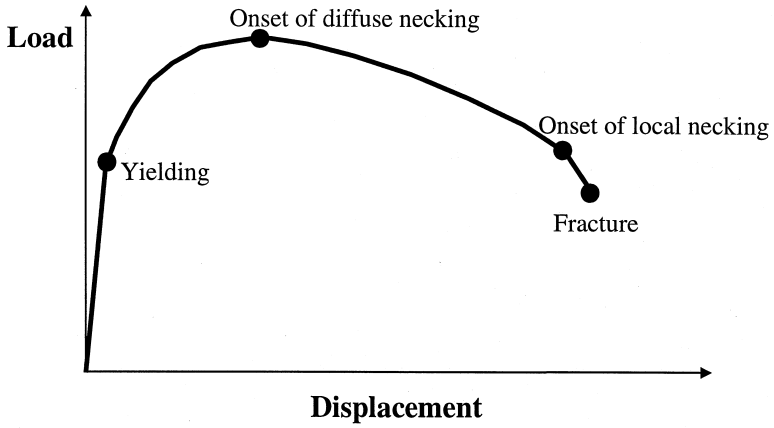

Fig. 2. Schematic plot of the load–displacement record of a tension test.

test. Uniform elastic–plastic deformation stops at the onset of diffuse necking, followed by non-uniform plastic deformation. The process from the onset of local necking to fracture is often a very short and rapid process. This investigation focuses on the non-uniform flow process from the onset of diffuse necking to the onset of local necking. The proposed equations cease to be valid when the localized neck starts to develop.

In this study, an extensive three-dimensional (3-D) numerical study on the diffuse necking behaviour of rectangular tensile specimens with various aspect ratios and plastic strain hardening ability has been carried out. Isotropic homogeneous materials are considered. It is shown that the area reduction can be separated into two parts, the proportional area reduction calculated directly from the thickness reduction and the non-proportional reduction due to shape change of the cross-section. The total area reduction deviates from the proportional part once the diffuse necking starts, just after the maximum load. Numerical results show that the area reduction due to shape change can be approximately normalized by the cross-section aspect ratio and the strain at the maximum load, which represents materials plastic hardening ability. After the true area reduction has been calculated, the true stress–logarithmic strain curve can be obtained.

It has been found that for the same material, before the local necking all the specimens with different aspect ratios give exactly the same true average stress–logarithmic strain curves as a round tensile bar. Therefore, the Bridgman equation can still be applied for the correction of true stress obtained from rectangular specimens for necking.

In the following, the numerical procedure used in the study, including the finite element models and materials, is reported first. The diffuse necking behaviour is briefly discussed in Section 3. Then an approximate relation between the thickness reduction and the total area reduction for different materials and aspect ratios is presented in Section 4. In Section 5, the relation was verified by comparing the true stress–strain curve calculated according to the proposed procedure using the load–thickness reduction relation and the 'exact' curve directly obtained from the finite element analyses for various kinds of materials. The Bridgman correction for the true stress–strain curve is examined in Section 6. A procedure for determining true stress–strain from rectangular tensile specimens in proposed in the final part of the paper. The limitation of the method is also discussed. The scope of the work carried out in this paper is schematically shown in Fig. 3.

2. Numerical procedure

2.1. Finite element models

Figure 4(a) shows the typical mesh (1/8) for the tensile specimen with rectangular cross-section. The initial thickness of all the specimens, t_0, is fixed. Specimens with initial aspect ratio $S = w_0/t_0 = 1$–5, 8 have been analyzed. The initial length of the specimens with aspect ratio 1–5 is fixed to $L_0 = 24t_0$. The length of the specimen with aspect ratio 8 is $L_0 = 40t_0$, in order to have sufficient length/width ratio. Because only the diffuse necking is concerned in this study, by making use of the symmetries with all the three co-ordinate planes one eighth of the specimen was modeled. There are four 3-D 8-node brick elements in half of the thickness and 12 elements in half of the width. The mesh in the length direction is biased with fine mesh close to the centre of the specimen. There are 640 3-D elements and 935 nodes in the model with aspect ratio 4. The meshes for other

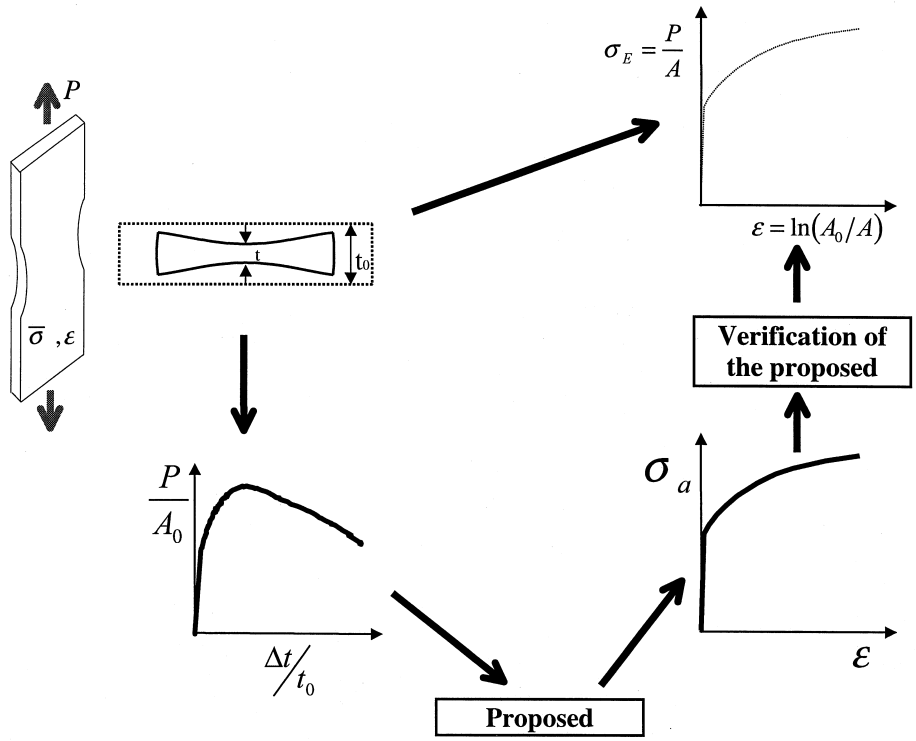

Fig. 3. Schematic plot of the scope of the study: from the FE analysis we can obtain both the load–thickness reduction curve and the 'exact' true stress–strain curve, $\sigma_E - \varepsilon$; a method is proposed to calculate the approximate true stress–strain curve, $\sigma_a - \varepsilon$, from the load–thickness reduction curve; this method is verified by comparing the approximate and 'exact' true stress–strain curves.

specimens with different aspect ratios are in general similar to the mesh shown in Fig. 4(a). The actual number of elements in the width direction is adjusted according to the absolute value of the width. The effect of mesh size and Gauss integration scheme on the loading behaviour of rectangular tensile specimen has been investigated by Tvergaard (1993) and very limited effect was observed. Compared with other notched or cracked specimens the stress distribution in the tensile specimen is relatively uniform even after the diffuse necking has appeared. Therefore, we can expect that the current meshes employed in the computations may be fine enough.

Because only diffuse necking is concerned in this study, the displacement boundary conditions applied to the model are defined as follows:

$$\begin{aligned} &y = L_0/2: \quad u_y = u_{\text{prescribed}}, \\ &y = 0: \quad u_y = 0, \\ &x = 0: \quad u_x = 0, \\ &z = 0: \quad u_z = 0. \end{aligned} \tag{1}$$

In order to trigger necking, an initial imperfection, 0.4% of the width with a notch radius $12t_0$

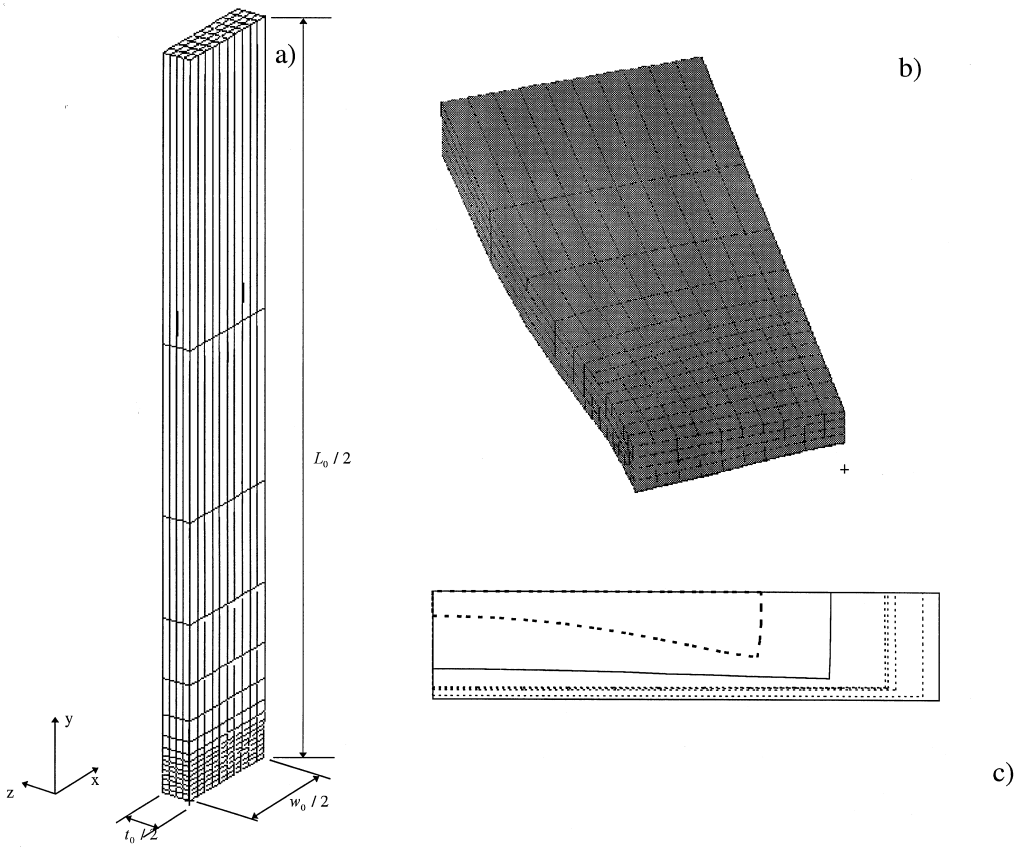

Fig. 4. (a) Finite element mesh (1/8) for the model with aspect ratio 4, (b) symmetrical necking for specimen with aspect ratio 4, hardening exponent 0.15, $E/\sigma_y = 500$, and (c) shape change of the cross-section (1/4).

is applied to both sides in the width direction in the centre of the model. Preliminary study with different values of the imperfection has shown that the applied initial imperfection has little influence on the numerical results. A similar observation was noted by Tvergaard (1993).

2.2. Materials

Materials with various hardening behaviour have been analyzed. The materials in general can be classified into two categories, the one with which the hardening behaviour can be described by a single parameter, for example, the hardening exponent according to a power hardening law and the one its hardening behaviour cannot be described by a single parameter. In this study, materials with the following rate-independent strain hardening power law have been analyzed first:

$$\bar{\sigma} = \sigma_0 \left(1 + \frac{\bar{\varepsilon}_p}{\varepsilon_0}\right)^n, \tag{2}$$

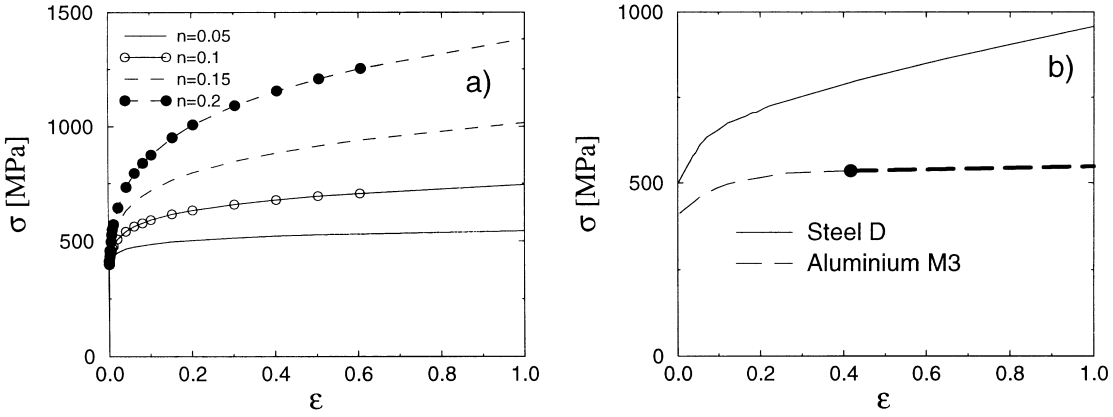

Fig. 5. (a) The materials used for deriving the area–thickness reduction relation. Shown in the figure are the materials with different hardening exponents and $E/\sigma_y = 500$ and $v = 0.3$, (b) the two real materials used for testing the area–thickness reduction relation. In (b) the bold dashed line after the dot is artificially extrapolated.

where $\bar{\sigma}$ is the flow stress corresponding to the equivalent plastic strain $\bar{\varepsilon}_p$, σ_0 is the yield stress, ε_0 is the yield strain $\varepsilon_0 = \sigma_0/E$, n is the strain hardening exponent and E the Young's modulus. Four hardening exponents, $n = 0.05$, 0.1, 0.15 and 0.2 with $E/\sigma_y = 500$ and Poisson ratio $v = 0.3$ have been considered. One calculation with $n = 0.15$, $E/\sigma_y = 175$ and $v = 0.3$, has also been carried out. From the results of this type material, the approximate relation between the area reduction and thickness reduction for determining the true stress–logarithmic strain curve was established.

The established method was then tested by applying the method to two real materials, one steel and one aluminium, for which the hardening behaviour cannot be described by a single parameter. Figure 5(a) shows the materials with $E/\sigma_y = 500$, $n = 0.05$, 0.1, 0.15 and 0.2 and Fig. 5(b) the two real materials, steel D (see Zhang and Hauge, 1995) and aluminium M3 (Ødegård and Zhang, 1997).

The analyses were performed by using large deformation and incremental plasticity theory implemented by ABAQUS. Each run with extensive output takes approximately one hour CPU time in a CRAY J90 computer. By combining different material and cross-section aspect ratios, totally 48 analyses have been performed.

3. Diffuse necking

The main concern of this study is to determine the true stress–strain curve from the diffuse necking mode (symmetrical) of tensile specimens with rectangular cross-section. The assumed boundary conditions, symmetries and initial imperfections guarantee that the diffuse necking rather than the local necking appears first critical. According to the Considere (1885) criterion, the onset of necking occurs when the true hardening rate exactly equals the true stress, just after the maximum load:

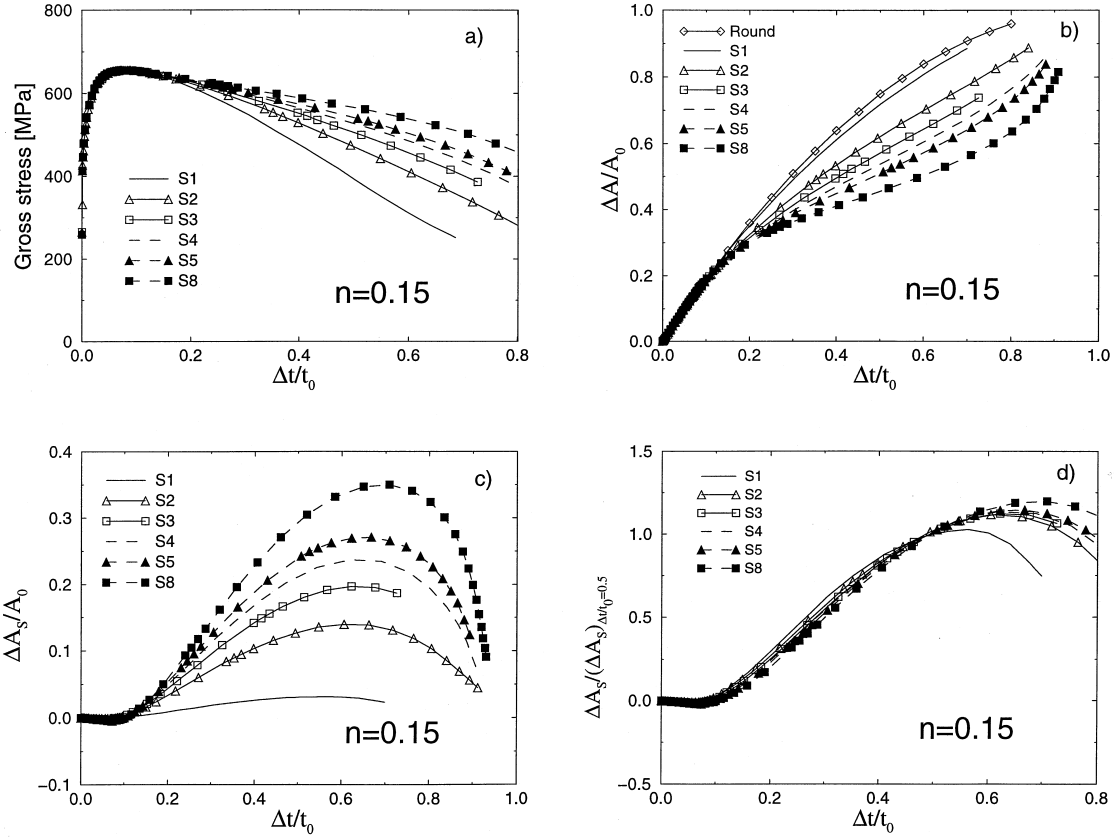

Fig. 6. (a) Gross stress vs thickness reduction, (b) total area reduction vs thickness reduction, (c) non-proportional area reduction vs thickness reduction and (d) normalized curves of (c) by the corresponding non-proportional area reduction at 50% thickness reduction. The material is $n = 0.15$, $E/\sigma_y = 500$ and $v = 0.3$.

$$\frac{d\sigma}{d\varepsilon} = \sigma. \tag{3}$$

Figure 6(a) shows the gross stress vs thickness reduction curves for the material with hardening exponent $n = 0.15$, obtained from the finite element analyses for various aspect ratios. For the material model shown by eqn (2), we obtain the strain at the maximum load at $\varepsilon = 0.15$, which corresponds to 7.5% of thickness reduction. The maximum load in the analyses appears very close to the 7.5% thickness reduction. This observation is the same for all the aspect ratios. The exact value is slightly influenced by the value of the initial imperfection and the load increment scheme. It can be seen from Fig. 6(a) that after the maximum load, the load decreases much faster in the specimens with low aspect ratio than with high aspect ratio.

Figure 4(b) shows the deformed mesh for the model with aspect ratio 4 and 4(c) for the original and deformed minimum cross-section. Although there is a tendency for local necking in later stage

especially for low hardening material, the minimum area appears in the centre of the specimen in all the analyses, where the thickness reduction is recorded. This certifies that the recorded thickness reduction is the reduction at the minimum section. The check is performed for all the analyses to guarantee a valid load thickness reduction curve.

4. Thickness reduction and area reduction of rectangular cross-section

4.1. Proportional and non-proportional area reduction

Necking according to the Considere criterion appears just after the maximum load. The deformation before the necking is uniaxial and the reduction of the cross-section is purely due to proportional area change. However, unlike the round tensile bar, the shape of the cross-section of rectangular specimen will change once the necking starts, see Fig. 4(c). Therefore, the total area reduction ratio of a rectangular tensile specimen at the minimum cross-section can be separated into a proportional part calculated from the thickness reduction and another non-proportion part due to shape change:

$$\frac{\Delta A}{A_0} = \frac{\Delta A_P}{A_0} - \frac{\Delta A_S}{A_0} \tag{4}$$

where the first part is the same as a round bar and can be easily written:

$$\frac{\Delta A_P}{A_0} = 2\left(\frac{\Delta t}{t_0}\right) - \left(\frac{\Delta t}{t_0}\right)^2. \tag{5}$$

The curves of total area reduction vs thickness reduction for $n = 0.15$ are shown in Fig. 6(b) for all the aspect ratios analyzed. A special numerical procedure for calculating the 'exact' total area from the deformation of the boundary nodes outputted from finite element analysis was used. In the figure, eqn (5) which represents the relation for a round bar is also plotted. We observe that the curves for the rectangular specimens deviate from the proportional area reduction, eqn (5), just after the maximum load. In general, tensile specimen with square cross-section is very close to proportional area change. The larger the aspect ratio, the larger the deviation from the proportional area reduction.

The non-proportional area reduction ratio due to shape change $\Delta A_S/A_0$, has been plotted in Fig. 6(c). From this figure we can observe clearly the point where non-proportional area reduction starts. Figure 6(c) shows that the non-proportional area reduction reaches a maximum at about 70% of thickness reduction, then decreases. This means that the total area reduction becomes more proportional with the increase of thickness reduction after this maximum.

It should be noted that this may not have much practical meaning and could be a purely artificial behaviour, because local necking in engineering alloys may appear and terminate the loading, far before the maximum non-proportional area reduction has reached. As will be explored later on, the maximum valid range of thickness reduction ratio in this study is limited to 50% of the initial thickness so that the reduction ratio beyond 50% is not taken into consideration.

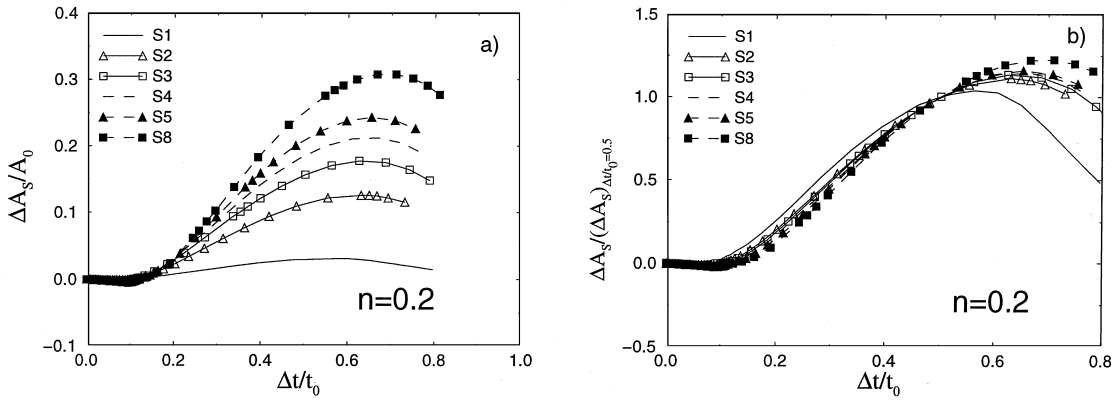

Fig. 7. (a) Non-proportional area reduction vs thickness reduction and (b) normalized curves of (a) by the corresponding non-proportional area reduction at 50% thickness reduction. The material is $n = 0.1$, $E/\sigma_y = 500$ and $\nu = 0.3$.

4.2. Normalization of the non-proportional area reduction with respect to section aspect ratio

By examining the shapes of the curves in Fig. 6(c), we notice that they are very similar to each other before the maximums. It has therefore been tried to find whether the curves of different aspect ratios can be normalized. By taking out the non-proportional area reduction at 50% thickness reduction and normalizing the curves in Fig. 6(c) by these values, we obtain a new set of curves which are shown in Fig. 6(d).

Interestingly, all the curves approximately collapse into one in the range $\Delta t/t_0 \leqslant 0.5$, especially for the aspect ratios greater than one. In contrast, the normalized curve for the specimen with square cross-section deviates slightly from the curves with larger aspect ratios. The reason for this behaviour is not quite clear to the authors, it maybe due to the very small non-proportional area reduction (see Fig. 6(b), (c)) that the present mesh for the specimen with square cross-section is not fine enough.

The non-proportional area reduction vs thickness reduction and the corresponding normalized curves for the material with $n = 0.2$, 0.1 and 0.05 are shown in Figs 7–9, respectively. Similar behaviour as Figs 6(c) and (d) is observed. Comparing Figs 6–9, it can be seen that non-proportional area reduction starts early for low hardening material. Furthermore, for a given thickness reduction, the corresponding non-proportional are reduction for a low hardening material is larger than that for a strong hardening material. This implies that soft material tends to have large shape change.

Figure 6–9 show that for the materials investigated, the non-proportional area reduction vs thickness reduction for different aspect ratios can be normalized by the non-proportional area reduction at 50% of thickness reduction.

Figure 10(a) shows the non-proportional area reductions corresponding to 50% of thickness reduction, used for the normalization in Figs 6–9, as a function of the aspect ratio for the four materials analyzed. Figure 10(b) is a new set of curves of Fig. 10(a), by normalizing the curves by the corresponding values of aspect ratio 4. Interestingly, the curves for the four materials collapse into one especially for aspect ratio less than eight. This normalization indicates that for any

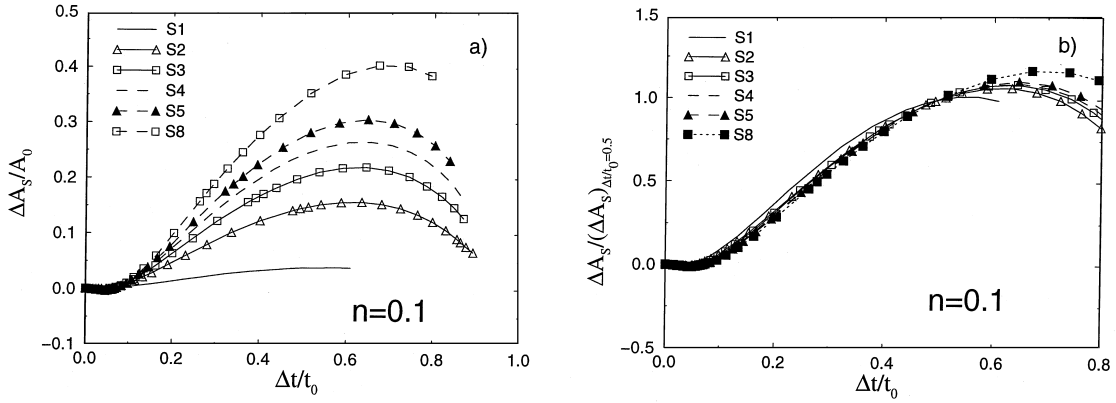

Fig. 8. (a) Non-proportional area reduction vs thickness reduction and (b) normalized curves of (a) by the corresponding non-proportional area reduction at 50% thickness reduction for the material with $n = 0.1$, $E/\sigma_y = 500$ and $v = 0.3$.

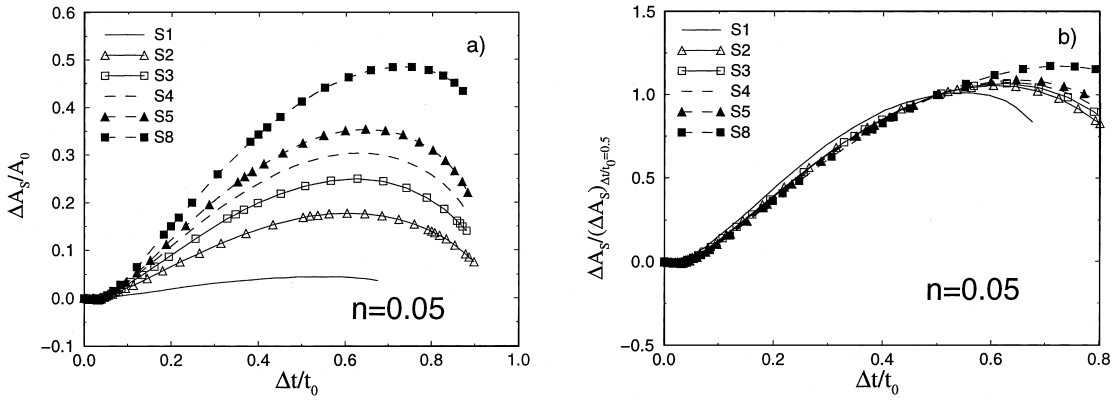

Fig. 9. (a) Non-proportional area reduction vs thickness reduction and (b) normalized curves of (a) by the corresponding non-proportional area reduction at 50% thickness reduction for the material with $n = 0.05$, $E/\sigma_y = 500$ and $v = 0.3$.

material, the value of non-proportional area reduction at 50% thickness reduction for any aspect ratio can be predicted from the corresponding value for aspect ratio 4.

4.3. Normalization with respect to the strain at maximum load

From Figs 6(d), 7(b), 8(b) and 9(b), we observe that the non-proportional area reduction starts at different thickness reduction ratios for different materials, see Fig. 11(a) for aspect ratio 4. However, the shape of the normalized curves in the net thickness reduction range, $\Delta t/t_0 - (\Delta t/t_0)_{P_{max}}$, looks very similar to each other.

Regarding this observations, the four curves in Fig. 11(a) have been plotted in Fig. 11(b) with the following transformation:

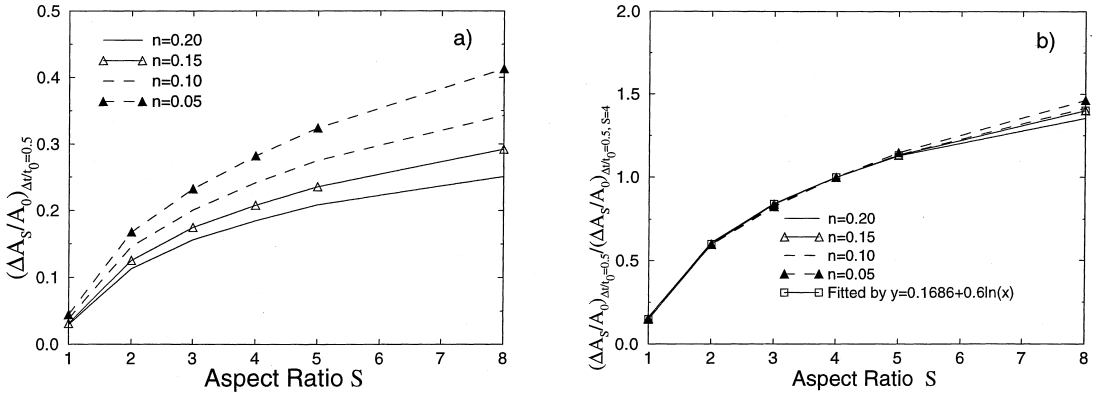

Fig. 10. (a) The quantities used in the normalization of Fig. 6(c), 7(b), 8(b) and 9(b) as a function of aspect ratio S for the four materials and (b) new set of curves by dividing the curve for each material in (a) by the corresponding value for aspect ratio 4.

$$\frac{\Delta t}{t_0} = \frac{\Delta t}{t_0} - \left(\frac{\Delta t}{t_0}\right)_{P_{max}} + \left(\frac{\Delta t}{t_0}\right)^{n=0.15}_{P_{max}} . \tag{6}$$

The above transformation simply means that all the curves except the one for $n = 0.15$ are transformed to have the same value of thickness reduction at which the non-proportional area reduction starts as the one for the material $n = 0.15$. It can be seen that the four curves do not collapse into one. Using the same normalization procedure as used in the Figs 6(d), 7(d), 8(b) and 9(b), the four curves collapse into one in Fig. 11(c). Figure 11(d) shows the normalized non-proportional area reduction for material $n = 0.15$ vs net thickness reduction. The quantities used for the normalization in Fig. 11(c), $(\Delta A_S/A_0)^T_{\Delta t/t_0=0.5}$, where the superscript T represents the transformed curves, are plotted as a function of the corresponding thickness reduction at the maximum load in Fig. 12. An approximate linear relation is shown.

4.4. Proposed area reduction equation

Figures 11 and 12 show that different material differs in $(\Delta t/t_0)_{P_{max}}$. However, when the non-proportional area reduction vs thickness reduction curves are transformed to the same thickness reduction at which necking starts, the curves can be normalized by the quantities which are a linear function of the $(\Delta t/t_0)_{P_{max}}$—the material parameter. The normalized curve is only a function of the net thickness reduction, $\Delta t/t_0 - (\Delta t/t_0)_{P_{max}}$, see Fig. 11(d).

Figure 11 indicates that the non-proportional area reduction curves for different materials but same cross-section can be normalized by the net thickness reduction after the maximum load. From the above observation and be recalling Fig. 10(b) that for the same material the non-proportional area reduction vs thickness reduction for an aspect ratio can be derived from another, we can derive the following equation for calculating the non-proportional area reduction:

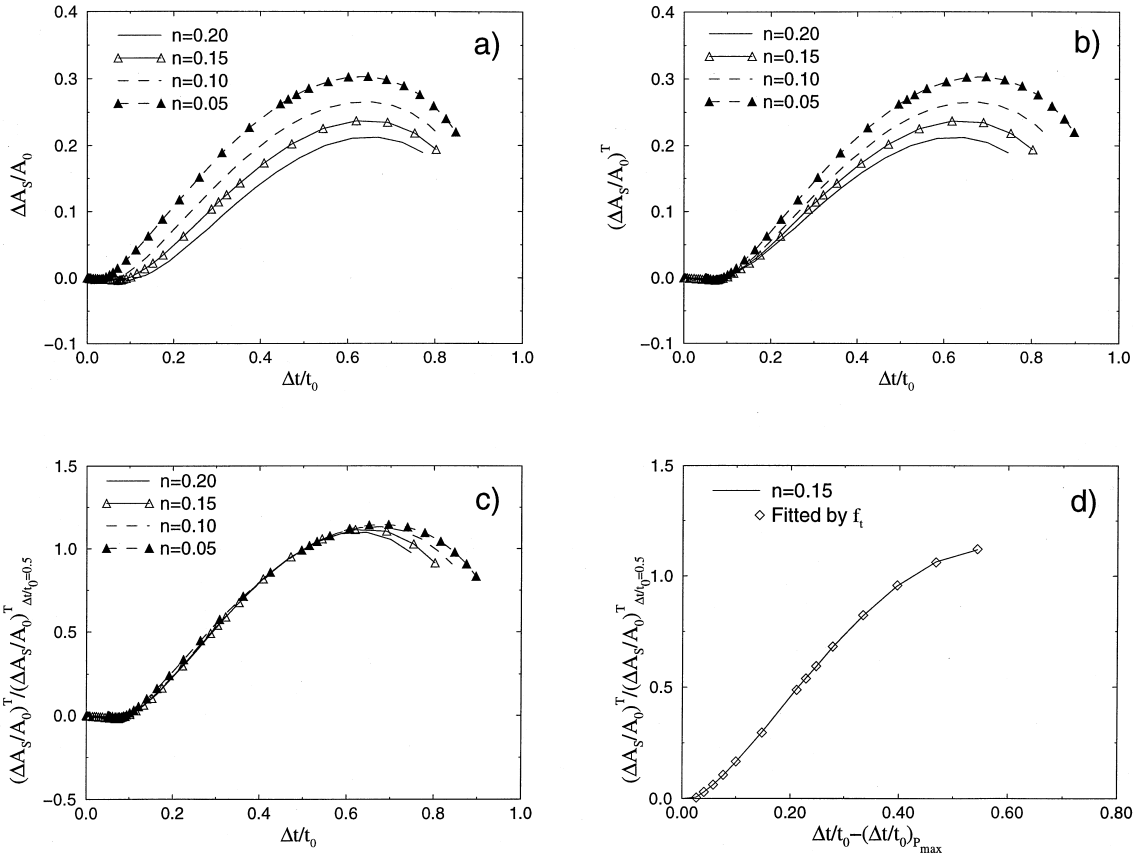

Fig. 11. (a) Non-proportional area reduction vs thickness reduction for the four materials with aspect ratio 4; (b) transformed according to eqn (6) to the same thickness reduction at which the non-proportional area reductions starts as that of material with $n = 0.15$; (c) normalized curves of Fig. 11(b) by the values at 50% reduction thickness; (d) normalized non-proportional area reduction for $n = 0.15$ vs net thickness reduction.

$$\left(\frac{\Delta A}{A_0}\right)_S = f_s(S) f_t\left(\frac{\Delta t}{t_0} - \left(\frac{\Delta t}{t_0}\right)_{P_{max}}\right) f_m\left(\left(\frac{\Delta t}{t_0}\right)_{P_{max}}\right). \tag{7}$$

The above equation includes three parts: the first part is dependent on the aspect ratio. In this study, the aspect ratio 4 has been chosen as the reference aspect ratio, therefore, $f_s(4) = 1$. For any other aspect ratio, the following equation has been fitted from Fig. 10(b),

$$f_s(S) = 0.1686 + 0.6\ln(S). \tag{8}$$

The second part is a distribution of the non-proportional area reduction vs the net thickness reduction (the total thickness reduction minus the reduction at the maximum load) which is fitted from Fig. 11(d),

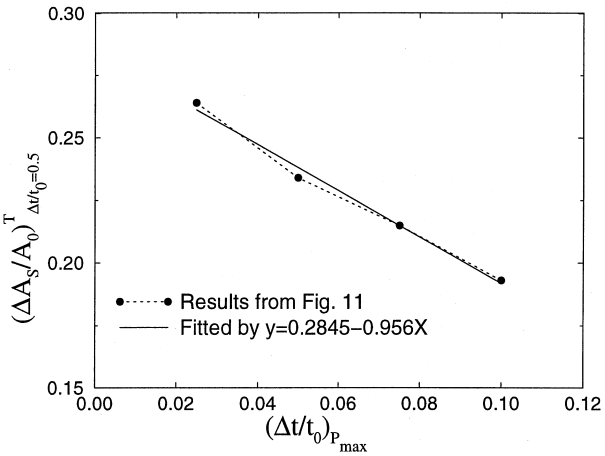

Fig. 12. Quantities used in the normalization of Fig. 11(c).

$$f_t(x) = c_0 + c_1 x + c_2 x^2 + c_3 x^3 + c_4 x^4 \tag{9}$$

where $x = (\Delta t/t_0) - (\Delta t/t_0)_{P_{max}}$ and the constants are

$$\begin{aligned} c_0 &= -0.03069 \\ c_1 &= 1.09016 \\ c_2 &= 11.1512 \\ c_3 &= -25.1 \\ c_4 &= 14.8718. \end{aligned} \tag{10}$$

The first and second parts are geometric factors, while the third part of eqn (7) is material specific. In eqn (7), the material hardening effect on the non-proportional area reduction is characterized by one material parameter, $(\Delta t/t_0)_{P_{max}}$. The validity of the approach is discussed in the final part of the paper. From Fig. 12 a linear equation is fitted:

$$f_m = 0.2845 - 0.956 \left(\frac{\Delta t}{t_0}\right)_{P_{max}}. \tag{11}$$

From eqns (4) and (7) we can see that the total area reduction is a function of the aspect ratio and the thickness reduction. Once the load–thickness reduction curve is recorded for any specimen with rectangular cross-section, the area reduction can be readily calculated according to the proposed equations.

Combining eqns (4) and (7) we can write the complete area reduction equation,

$$\frac{\Delta A}{A_0} = 2\left(\frac{\Delta t}{t_0}\right) - \left(\frac{\Delta t}{t_0}\right)^2 - f_s(S) f_t\left(\frac{\Delta t}{t_0} - \left(\frac{\Delta t}{t_0}\right)_{P_{max}}\right) f_m\left(\left(\frac{\Delta t}{t_0}\right)_{P_{max}}\right). \tag{12}$$

In general the area reduction equation can be written

$$\frac{\Delta A}{A_0} = f\left(\frac{\Delta t}{t_0}, S, \left(\frac{\Delta t}{t_0}\right)_{P_{max}}\right). \tag{13}$$

5. Verification of the area reduction formula

5.1. 'Exact' true stress–strain curves

Before verifying the area reduction equation (12) the 'exact' true average stress–logarithmic strain curves calculated directly from the finite element analyses with different aspect ratios are compared. Figure 13(a) shows the results for the material $n = 0.2$. The results from the analysis of round tensile specimen using the mesh shown in Fig. 13(b) are also presented. Specimens with different aspect ratios give exactly the same true average stress–logarithmic strain curves as the round specimen. This behaviour is the same for all the other materials. The results in Fig. 13(a) means that materials true stress–strain curve can be actually determined from either the round specimen or rectangular tensile specimen, as long as the area reduction can be measured.

5.2. Comparison of the 'exact' and approximate true stress–strain curves

The proposed area reduction equation eqn (12) has been verified by comparing with the 'exact' area reduction directly calculated from the finite element analyses. The input for calculating the area reduction using eqn (12) is the load–thickness reduction curve obtained from the finite element analyses. Figure 14(a) shows the results for the material with $n = 0.2$. The calculation by using eqn (12) stops when the thickness reduction is greater than 50%. The logarithmic strain calculated as, $\varepsilon = \ln(A_0/A)$, is limited to 100% in the presentation of Figs 14 and 15, which should be sufficient for most of the cases. We observe that the true average stress–logarithmic strain curves for all the aspect ratios calculated by using eqn (12) fits exactly with the 'exact' curve obtained directly from the finite element analyses, for the aspect ratio 4. The comparison for the material $n = 0.05$ is shown in Fig. 14(b). The results by using eqn (12) agree well with the finite element results except slightly worse agreement for the case with aspect ratio 8. This is due to the fact that local necking tends to appear quite early even in the boundary conditions defined by eqn (1) for this low hardening material with aspect ratio 8.

The proposed area reduction equation has been verified against the material with $n = 0.15$, $E/\sigma_y = 175$ and $\nu = 0.3$, and also the materials which cannot be described by a single power hardening law in Fig. 15(a) for the steel and Fig. 15(b) for the aluminium. Very satisfactory agreement is seen in the comparison.

6. Necking correction for the true stress

As it is obvious that the stress distribution across the cross-section is not uniform and triaxial stress starts to develop once the necking appeared, the calculated true stress is in an average sense and should be corrected due to the non-uniform distribution in the neck. The real stress distribution across the cross-section is very complicated. Arnofsky (1951) attempted to calculate the neck stress

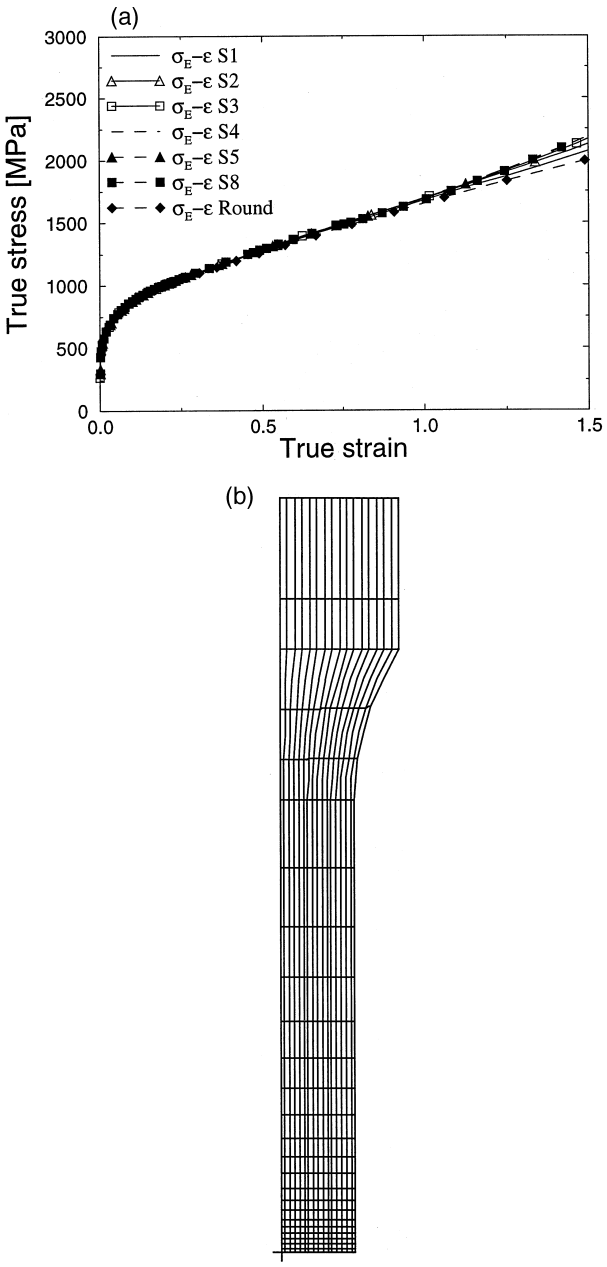

Fig. 13. (a) 'Exact' true stress–logarithmic strain curves of a round specimen and specimens with different aspect ratios, (b) mesh used for the round specimen (1/4).

from the measured strain and the true stress strain relation determined from the round specimen made of the same material. However, Fig. 13 shows that as long as the true area reduction can be calculated, the specimens with various aspect ratios give exactly the same true average stress–

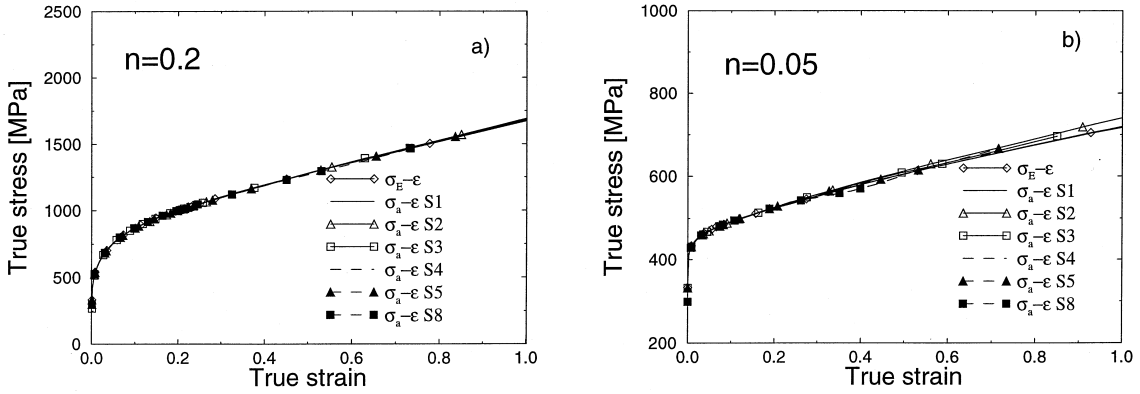

Fig. 14. (a) Comparison of the true stress–strain curve calculated from the proposed area reduction equation and directly from the finite element analyses for the material with $n = 0.2$ and (b) for the material with $n = 0.05$.

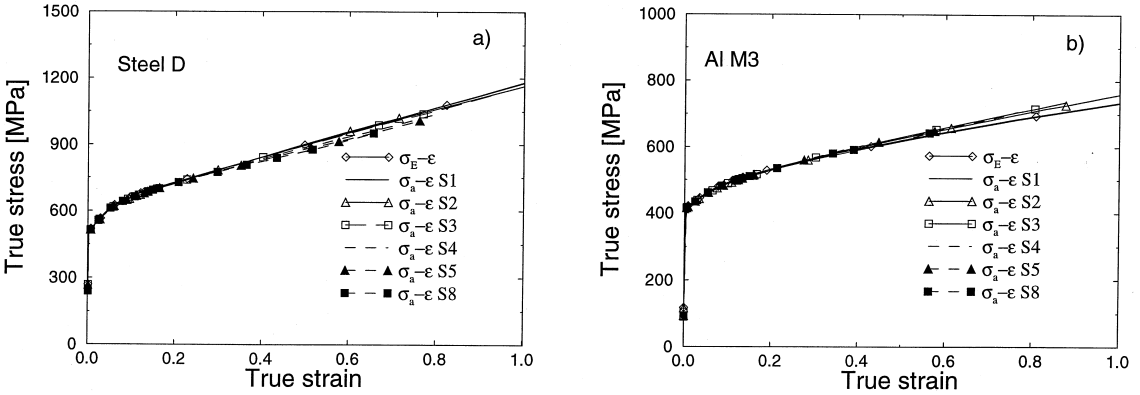

Fig. 15. (a) Comparison of the true stress–strain curve calculated from the proposed area reduction equation and directly from the finite element analyses for the steel D and (b) for the aluminium M3. Both materials cannot be described by one single hardening parameter.

logarithmic strain curves. That means that the same procedure used for the round tensile specimen can be 'equivalently' used for the correction of the true stress obtained from rectangular tensile specimen, without going to details of the stress distribution. For the round tensile specimen, the following correction equation by Bridgman (1952) is well known:

$$\frac{\sigma_b}{\sigma} = 1 \Big/ \left(\left(1 + \frac{2R}{a} \right) \ln \left(1 + \frac{\sigma}{2R} \right) \right) \tag{14}$$

where a is the current radius of the neck and R is the radius of curvature of the neck surface in the longitudinal plane at the minimum section. The correction starts once the maximum load has passed.

The difficult part in the application of the Bridgman correction is the determination of the neck

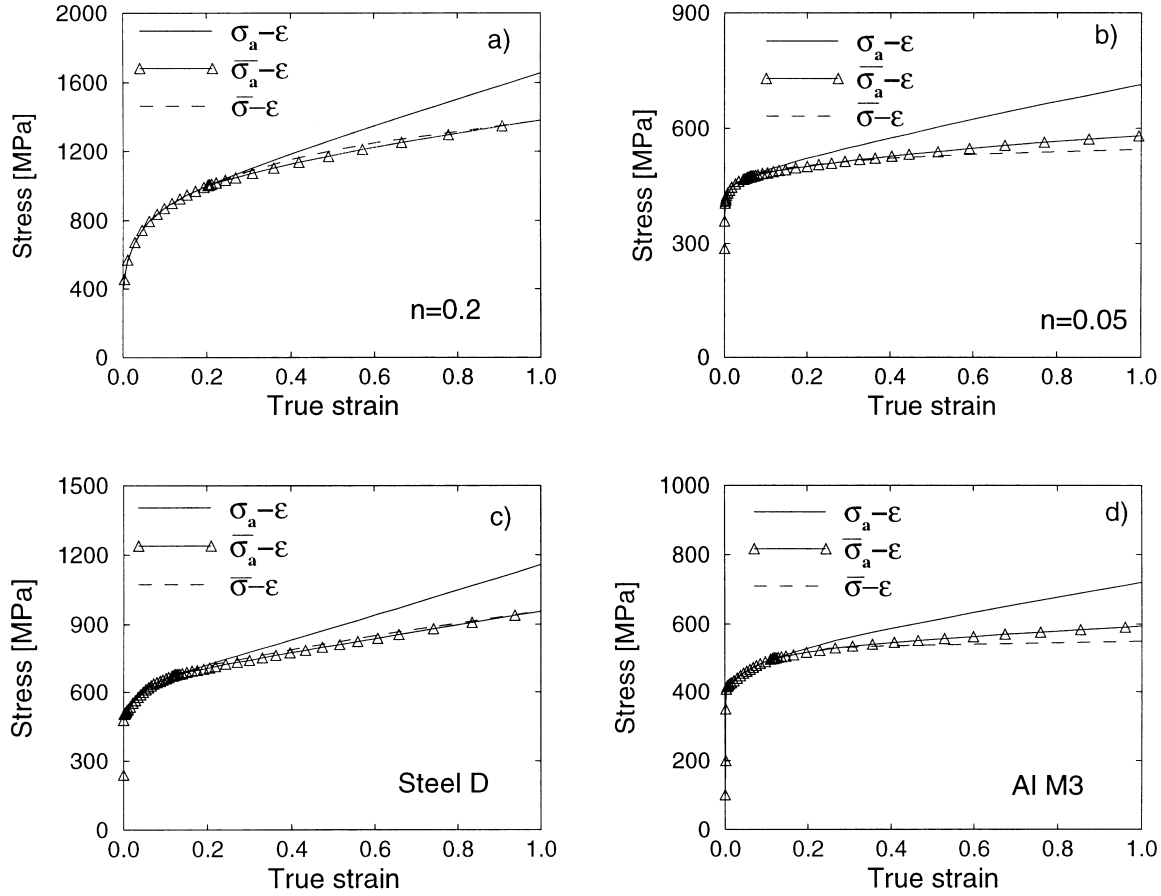

Fig. 16. Bridgman–Le Roy correction for (a) material with $n = 0.2$, (b) with $n = 0.05$, (c) steel D and (d) aluminium M3.

geometry parameter, the value of a/R. Le Roy et al. (1981) have presented an empirical expression for the neck geometry parameter:

$$\frac{a}{R} = 1.1(\varepsilon - \varepsilon_{P_{max}}). \tag{15}$$

The above equation has been examined for all the materials considered in the paper. The results for the material with $n = 0.2$, $n = 0.05$ and the two real materials are shown in Fig. 16. Reasonably good results are observed.

7. Proposed procedure and discussions

The main findings from numerical calculations carried out in the paper can be summarized as follows:

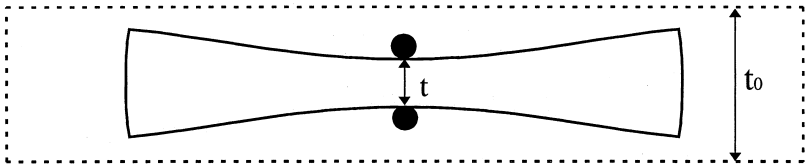

Fig. 17. Location for measuring the thickness reduction.

For same material, the non-proportional area reduction vs thickness reduction for different aspect ratios can be normalized by the value at 50% thickness reduction. Furthermore, for any material, the quantities used for the normalization can be described by an unique equation of aspect ratio. For different materials with same aspect ratio, the area reduction due to shape change vs net thickness reduction curves can be normalized by quantities which are a linear function of the thickness reduction at the maximum load.

By summarizing the results, the following procedure for determining the true stress–strain curve from rectangular specimens is proposed:

Prepare tensile specimens with rectangular cross-section. The maximum aspect ratio of the cross-section is limited to eight. When aspect ratio larger than eight is used, there is no guarantee for valid large range true stress–strain curve by using the proposed equation eqn (12). The recommended aspect ratio for the rectangular cross-section is four.

An initial imperfection up to 0.4% in both sides of the width direction located in the central part of the specimen may be used to trigger diffused necking in the centre where the thickness reduction measuring device is positioned.

Perform the uniaxial test by recording the load and measuring the thickness reduction at the minimum section. Figure 17 shows the specified location for measuring the thickness reduction in the minimum cross-section plane.

Once a valid load vs thickness reduction curve for any material and any specimen with aspect ratio less than or equal to eight is obtained, eqn (12) can be used for calculating the true area reduction vs thickness reduction. The application of eqn (12) is straightforward because the thickness reduction at the maximum load can be easily found from the recorded load vs thickness reduction curve.

The true stress–strain curve can then be readily calculated using $\sigma = P/A$ and $\varepsilon = \ln(A_0/A)$, where A is the current area, A_0 is the initial area of the cross-section and P is the recorded load.

The true average stress should be corrected for necking. Because the true stress–strain curves determined from specimens with rectangular cross-sections are exactly the same as the one given by round tensile specimen, the Bridgman–Le Roy correction eqns (14)–(15) can be used for the necking correction of the true–strain curves from specimens with rectangular cross-section.

As mentioned early, only diffuse necking is considered in the paper. The validity of the proposed equations stop once a localized neck appears.

In this study, the aspect ratio of the cross-section has been limited to eight. Numerical results show that localized necking appears quite early already for the specimen with this aspect ratio and

low hardening ability $n = 0.05$, therefore, it is recommended to use specimens with small aspect ratio to determine the true stress–logarithmic strain curve.

The application of eqn (12) is limited to maximum 50% of the thickness reduction. The corresponding true strain is dependent on the aspect ratio. For small aspect ratio, more than 100% true strain can be obtained. Nevertheless, the range of true strain has been limited to 100% in all the analysis. This range should be considered sufficient for many practical applications.

Finally, it should be pointed out that only isotropic materials with Poisson ratio 0.3 have been considered in this study. Thus, the validity of the proposed equations is strictly limited to the above materials. An experiment procedure to verify the proposed method is going on. How to modify the present method for anisotropic materials has been investigated and will be published elsewhere (Zhang et al. (1998).

Acknowledgements

HRARC (Hydro-Raufoss Automotive Research Centre) is greatly appreciated for their financial support and the permission to publish this work. The work has also received support from the Research Council of Norway.

References

Aronofsky, J., 1951. Evaluation of stress distribution in the symmetrical neck of flat tensile bars. Journal of Applied Mechanics 18, 75–84.

Bayoumi, A.E., Joshi, R., 1992. On the formability/instability of stretch-forming sheet metals. Applied Mechanics Review 45, S154–S164.

Bridgman, P.W., 1952. Studies in Large Plastic Flow and Fracture. McGraw-Hill, New York.

Considere, A., 1885. Annales des Ponts er Chaussees IX9, 6 eme serie p. 574.

Dieter, D., 1986. Mechanical Metallurgy. McGraw-Hill, Singapore.

Le Roy, G., Embury, J.D., Edwards, G., Ashby, M.F., 1981. A model of ductile fracture based on the nucleation and growth of voids. Acta Metall. 29, 1509–1522.

Ødegård, J., 1997. Unpublished test report on the rectangular specimens of aluminium.

Ødegård, J., Zhang, Z.L., 1997. Quantification of damage parameters. SINTEF Report STF24 F97237.

Tvergaard, V., 1993. Necking in tensile bars with rectangular cross-section. Computer Methods in Applied Mechanics and Engineering 103, 273–290.

Zhang, Z.L., Hauge, M., 1995. Ramberg–Osgood parameter fitting for ACCRIS steels. SINTEF Memo.

Zhang, Z.L., Ødegård, J., Svik, O.P., 1998. Determining the true stress–strain curve for anisotropic materials with rectangular tensile specimen, in preparation.